www.czasopisma.pan.pl PAN POLSKA AKADEMIA NAUK www.journals.pan.pl

ARCHIVES OF ELECTRICAL ENGINEERING VOL. 68(1), pp. 173–183 (2019)

DOI 10.24425/aee.2019.125988

Measurement and simulation of a rotational single sheet tester

FABIAN MÜLLER, GREGOR BAVENDIEK, BENEDIKT SCHAUERTE, KAY HAMEYER

RWTH Aachen University, Institute of Electrical Machines, Germany
e-mail: fabian.mueller@iem.rwth-aachen.de

(Received: 19.09.2018, revised: 25.10.2018)

Abstract: The accurate prediction of iron losses has become a prominent problem in electromagnetic machine design. The basis of all iron loss models is found in the spatial field-locus of the magnetic flux density ($\boldsymbol{B}$) and magnetic field ($\boldsymbol{H}$). In this paper the behavior of the measured BH-field-loci is considered in FEM simulation. For this purpose, a vector hysteresis model is parameterized based on the global measurements, which then can be used to reproduce the measurement system and obtain more detailed insights on the device and its local field distribution. The IEM has designed a rotary loss tester for electrical steel, which can apply arbitrary BH-field-loci occurring during electrical machine operation. Despite its simplicity, the proposed pragmatic analytical model for vector hysteresis provides very promising results.

Key words: finite element method, magnetic hysteresis, magnetization processes, soft magnetic material

1. Introduction

Non-oriented electrical steel is commonly used as flux-guiding material in rotating electrical machines. These materials vary strongly in terms of their magnetic properties and micro-structural consistency, and are primarily characterized by their loss at 50 Hz and 1.5 T. In addition, the maximum permeability, saturation polarization and a few characteristics, one-dimensional B-H-points are given by the manufacturer. As the spatial field-loci of the magnetic flux density and magnetic field partially strongly differ from the one-dimensional hysteresis curves, the measurement, analysis and modeling of vector hysteresis is required to support computational machine modeling and design [1–3]. To achieve these goals, a measurement device that allows the measurement of two-dimensional hysteresis at different frequencies and spatial pathways is put into operation [4]. A vector hysteresis model is parametrized for an fully processed industrial non-oriented laminated electrical steel. Identified model parameters and their simulation results are depicted to measurements. The next step, before proceeding to realistic electrical machines simulations, is to simulate the rotational single sheet tester (RSST), using the received vector hysteresis models in finite element method analysis.

www.czasopisma.pan.pl PAN POLSKA AKADEMIA NAUK www.journals.pan.pl

2. Rotational single sheet tester (RSST)

Figure 1 depicts the magnetic construction of the studied RSST. To allow magnetizations in any x and y-direction, the yokes form cross-shaped arms leaving only a small airgap to the fixed sample in the middle. The magnetic paths are collectively closed over the rectangular outer part of the yoke. The windings fixed on the four arms of the yoke deliver the required field to magnetize the sample. The magnetic flux density $\boldsymbol{B}$, which is measured by two orthogonal windings that are brought into the sample by drilled holes, is controlled by adjusting the excitation current. In addition, the magnetic field on the sample surface $\boldsymbol{H}_s$ is determined. Two H-coils per direction are mounted at a fixed distance below the sample. Based on the two measured magnetic field strengths at different distances from the sample, the vector field strength at the sample itself can be determined by extrapolation following (1) [5]. The measurement frequencies can be chosen between 3 Hz and 5 kHz.

$$\boldsymbol{H}_s = \boldsymbol{H}(0) = \frac{x_1\boldsymbol{H}(x_1) + x_2\boldsymbol{H}(x_2)}{x_1 - x_2}\,. \tag{1}$$

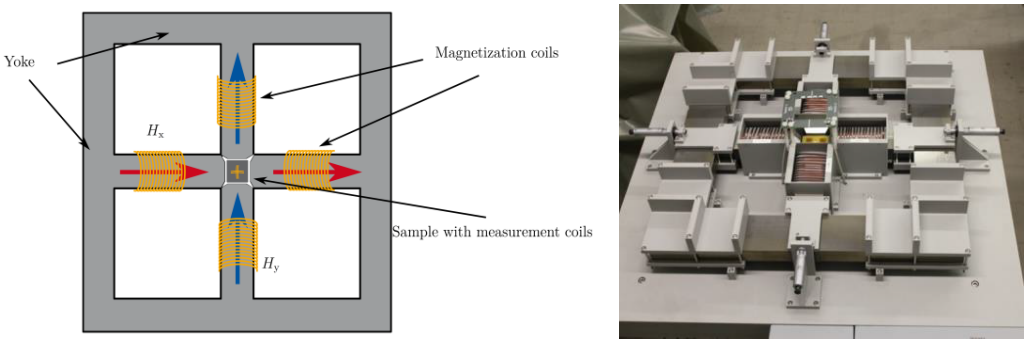

(a) (b)

Fig. 1. Topology (a) and picture (b) of utilized RSST-measurement system

The RSST enables unidirectional alternating magnetic measurements as well as circular and rotating magnetizations with different angles θ with respect to the RD-axis to reproduce the B-loci as they occur at different locations in electrical machines. Unidirectional loci that can be found inside the yoke are described by their amplitude $\hat{B}_{\mathrm{abs}}$ and their angle θ with respect to the rolling direction. Circular B-loci, as they appear between stator teeth and the yoke, are reproduced by a fixed amplitude that rotates with angular speed ω. Elliptical B-curves occur inside the stator teeth and are described by enhancing the circular B-loci by a factor for the axis ratio f_{Ax} and then a phase-shift of θ by a multiplication of a rotation matrix. The different applicable loci are shown schematically in Figure 2. The measurements were performed on a non-oriented electrical steel FeSi24-50A with a thickness of 0.483 mm and a silicon proportion of 2.4 wt%. The performed vector measurements at different circular excitations revealed next to a magnetic anisotropy, a considerable phase lag which depends on the respective saturation and current orientation of the magnetic flux density field vector. A thoroughly presentation of the rotational measurements of the material is given in [4].

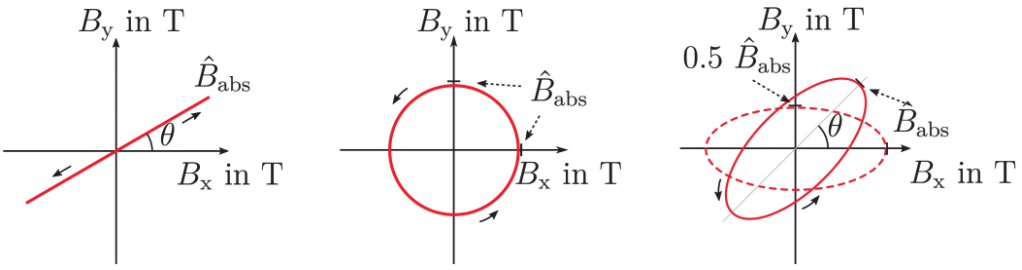

(a) (b) (c)

Fig. 2. Representation of different magnetic polarization curves the RSST can provide. A unidirectional B-loci with the angle θ with respect to RD (a); a circular B-loci (b) and an elliptical B-loci with axis ratio 0.5 and twisted main axis by θ (c) [1]

3. Vector hysteresis model

The vector hysteresis model utilized for the replication of the measured hysteresis curves and vector-field loci was originally proposed in [6] and represents a pragmatic approach to the replication of hysteresis curves and is abbreviated as PAM. The model is based on the homogenization of local material behavior descriptions on the mesoscopic scale. The static and dynamic behavior are considered in one mathematical expression using a set of five parameters for RD and TD. The reversible part of the magnetic field is represented by the first term of the equation and its parameters p_0, p_1 and p_2. The term forms a polynomial description of the anhysteretic saturation curve. The second term (p_3) corresponds to the additional field components caused by eddy currents and is related to the analytic description from Bertotti. The static hysteresis components of the magnetic field are taken into account by the last term (p_4 and p_5).

$$\boldsymbol{H}\left(p_k, \boldsymbol{B}, \dot{\boldsymbol{B}}\right) = \left(p_0 + p_1 \left|\boldsymbol{B}\right|^{2p_2}\right)\boldsymbol{B} + \left(p_3 + \frac{p_4}{\sqrt{p_5^2 + \left|\dot{B}\right|^2}}\right)\dot{\boldsymbol{B}}. \tag{2}$$

For the identified parameter set of the rolling direction the anhysteretic part and hysteretic part of the PAM are shown in Figure 3. Both curves are obtained through calculating the corresponding part of the hysteresis model, excited by a sinusoidal fluxdensity with an amplitude of 1.7 T and 50 Hz. While the anhysteretic part is of static nature (Figure 3(a)), the hysteretic part is dynamic (Figure 3(b)). The width of the hysteresis is determined by the time derivative of the magnetic flux density, resulting in a zero magnetic field strength, when the fluxdensity does not vary. This results in the advantage to be able to model frequency depending hysteresis curves. A thorough parameter study over a wider frequency range should be applied for a mean approximation. For simulation of hard magnetic hysteresis there are different approaches based on static hysteresis models or measurements [7].

It is possible to weight the dynamic parameters arbitrary, to achieve a more stable numerical model.

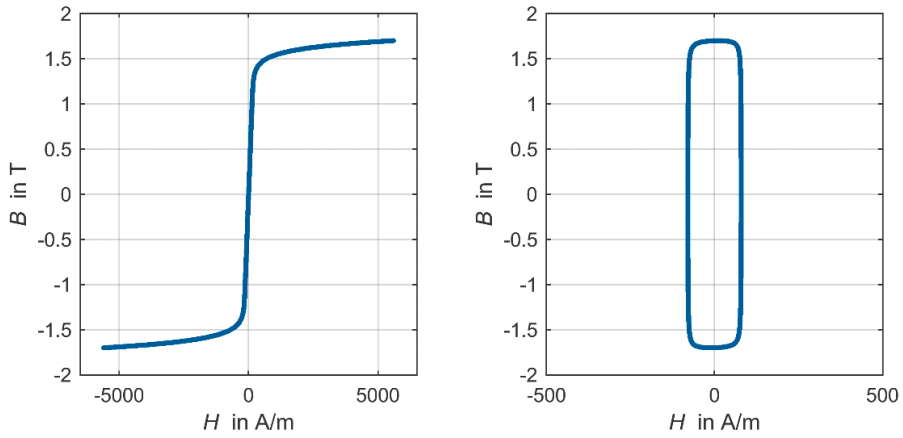

(a) Anhysteretic part (b) Hysteretic part

Fig. 3. Anhysteretic and hysteretic part of the PAM

For non-isotropic cases the formulation can be adjusted following:

$$\boldsymbol{H}_{x,y}\left(p_{k_{x,y}}, \boldsymbol{B}, \dot{\boldsymbol{B}}\right) = \left(p_{0_{x,y}} + p_{1_{x,y}} \left|\boldsymbol{B}\right|^{2p_{2x,y}}\right) \boldsymbol{B}_{x,y} + \left(p_{3_{x,y}} + \frac{p_{4_{x,y}}}{\sqrt{p_{5_{x,y}}^2 + \left|\dot{\boldsymbol{B}}\right|^2}}\right) \dot{\boldsymbol{B}}_{x,y} \,. \tag{3}$$

Two set of parameters $p_{kx,ky}$ are identified for each main-direction at unidirectional excitations at 50 Hz and 1.5 T peak flux density in the two main directions. Since the hysteretic field components are represented by two different terms. The identification is performed by error minimization methods between measurement and simulation and led to the following set of parameters:

Table 1. Identified parameter for unidirectional measurements of FeSi24-50A at 1.5 T

	p_0	p_1	p_2	p_3	p_4	p_5
RD	133.134	0.202	9.11	0	80.75	101.83
TD	578.458	5.15	5.944	0.0039	77.245	161.92

A large number of sophisticated approaches taking the vector properties of non-oriented electrical steel into account have been proposed in the past. Well known models are the vector Preisach [8] model and stop [9] or play [10] hysteresis models or the vectorized adjustments of analytical, parameter based originally one-dimensional approaches to model ferromagnetic hysteresis like the Jiles–Atherton model [11]. While the previously mentioned models require a large amount of measurements and computational resources for each machine element during finite element calculations, the latter depends in the quality of its outcomes on the step size and

www.czasopisma.pan.pl PAN POLSKA AKADEMIA NAUK www.journals.pan.pl

a gradual approach to the respective operating point. The comparatively unpretentious form of the chosen hysteresis model used in this work is intended to ensure a comparable low computational effort and ensure numerical stability in terms of an advantageous independency of the calculation step size during the numerical calculation in comparison to the mentioned approaches. Only the previous values of the field sizes are required for the stable calculation of the new operation point.

4. Finite element method

To consider vector-hysteretic behavior of ferromagnetic materials in the magnetic circuit and local effects like eddy currents, phase lags and anisotropy, the finite element method is used in combination with the PAM. The two-dimensional field problem is solved with a quasi-static magnetic vector potential formulation. The strong formulation, resulting from Amperes Law reads:

$$\nabla \times (\boldsymbol{\nu} \nabla \times \boldsymbol{A}) + \sigma \dot{\boldsymbol{A}} = \boldsymbol{J}. \tag{4}$$

The reluctivity $\boldsymbol{\nu}$ is a positive symmetric semidefinite tensor. Since the eddy current losses are included in the PAM, a quasi-static field problem is solved and the second term in (4) can be neglected in the hysteretic regions. The nonlinearity of the hysteretic material can be considered with two different methods; either a fixed-point method or a differential Newton method. The fixed-point method applied to the static A-formulation leads to (5) [12].

$$\nabla \times \left(\boldsymbol{\nu}_{FP} \nabla \times \boldsymbol{A}^{k} \right) = \boldsymbol{J} - \nabla \times \left(\boldsymbol{M}^{*}(\boldsymbol{B}) \right). \tag{5}$$

In eddy current regions, which do not consist of hysteretic material, the magnetoquasistatic formulation with application of the fixed-point method can be written as (6).

$$\nabla \times \left(\boldsymbol{\nu}_{FP} \nabla \times \boldsymbol{A}^{k} \right) + \sigma \dot{\boldsymbol{A}}^{k} = \boldsymbol{J} - \nabla \times \left(\boldsymbol{M}^{*}(\boldsymbol{B}) \right) + \sigma \dot{\boldsymbol{A}}^{k-1}. \tag{6}$$

$\boldsymbol{\nu}_{FP}$ is a tensor, which contains the fixed-point reluctivity on the main diagonal and the fixed-point reluctivity is optimally chosen to (7) [13].

$$\boldsymbol{\nu}_{FP\mathrm{opt}} = \left(\min \left(\boldsymbol{\nu}(\boldsymbol{B}) \right) + \max \left(\boldsymbol{\nu}(\boldsymbol{B}) \right) \right) \div 2. \tag{7}$$

$\boldsymbol{M}^{*}(\boldsymbol{B})$ is a magnetization-like quantity, which contains the information about the nonlinear materials [2] and can be expressed as:

$$\boldsymbol{M}^{*}(\boldsymbol{B})_{\mathrm{anhysteretic}} = \left(\boldsymbol{\nu}_{FP} - \boldsymbol{\nu}(\boldsymbol{B}) \right) \boldsymbol{B}, \tag{8}$$

$$\boldsymbol{M}^{*}(\boldsymbol{B})_{\mathrm{hysteretic}} = \boldsymbol{\nu}_{FP} \boldsymbol{B} - \boldsymbol{H}_{\mathrm{PAM}}(\boldsymbol{B}). \tag{9}$$

(8) is used to take care of linear, nonlinear and anisotropic material and the reluctivity holds the material behavior as a function of the magnetic flux density. In (9) $\boldsymbol{H}_{\mathrm{PAM}}$ is the magnetic field strength, calculated with the previously described dynamic vector-hysteresis model depending on the magnetic flux density. The fixed-point method has the advantage, that the convergence is guaranteed, as long as the field problem satisfy the condition of contraction mapping, but it needs more computation time, because of its linear convergence. Especially in regions with a low flux

www.czasopisma.pan.pl PAN POLSKA AKADEMIA NAUK www.journals.pan.pl

density amplitude many iterations can occur before reaching the convergence criterion [14, 15]. There are techniques to accelerate the fixed-point technique, according to information resulting from previous time steps in transient simulations [16].

The differential Newton method is the second approach to simulate the hysteretic material. It is applied by linearizing the equation on a given point by a first order tailor approximation and leads to (10).

$$P^k \cdot \Delta \boldsymbol{A}^k = \boldsymbol{J} - (\nabla \times \boldsymbol{H}(\boldsymbol{B})). \tag{10}$$

The magnetic field strength on the right side of the equation is derived by the material law or by the hysteresis model, depending on the material in the corresponding region. The Jacobian Matrix contains the information about the derivation of the nonlinearity in the working point [17].

$$\boldsymbol{\nu}_d = \frac{\partial \boldsymbol{H}}{\partial \boldsymbol{B}} = \begin{bmatrix} \partial H_x / \partial B_x & \partial H_x / \partial B_y \\ \partial H_y / \partial B_x & \partial H_y / \partial B_y \end{bmatrix}. \tag{11}$$

For isotropic non-hysteretic materials the Jacobian can be expressed as (12).

$$\frac{\partial \boldsymbol{H}}{\partial \boldsymbol{B}} = \frac{\partial \nu}{\partial \boldsymbol{B}^2} 2\boldsymbol{B}^2 + \nu. \tag{12}$$

The entries of the Jacobian Matrix in anisotropic and hysteretic regions can be obtained by (11), that can either be derived analytically or as a difference between two consecutive iterations (12), which is used in this article for the hysteretic regions [18].

$$\frac{\partial H_i}{\partial B_j} \approx \frac{H_{i,k} - H_{i,k-1}}{B_{j,k} - B_{j,k-1}} \quad \text{for} \quad i, j \in [x,\ y]. \tag{13}$$

The index k denotes the iteration step, if $k = 0$ the values of the previous time step are used. Due to numerical instabilities in some rare cases, only the main diagonal is filled with values unequal zero. The presented methods and hysteresis model are realised in the software package iMOOSE, developed by the Institute of Electrical Machines (IEM). To receive a unique solution for the finite element analysis the presented formulation is combined with the corresponding boundary conditions and the Coulomb Gauge (14), which is implicitly satisfied in two dimensional analysis.

$$\nabla \cdot \boldsymbol{A} = \frac{\partial A_z(x, y)}{\partial z} = 0. \tag{14}$$

5. Comparison of measurements and numerical simulation

To simulate the behavior of the previously presented measurement system, the RSST is built as a two-dimensional model, under the assumption that the stray fluxes in z-direction can be neglected. In Figure 4(a) the outline of the model is presented. It consists of a yoke with four teeth, two for each axis. The excitation coils are placed on the teeth with 45 turns each in correspondence to the actual measurement system. In Figure 4(b) the sample and its mesh, containing 5 355 elements, is pictured. For the two dimensional simulation first order nodal shape

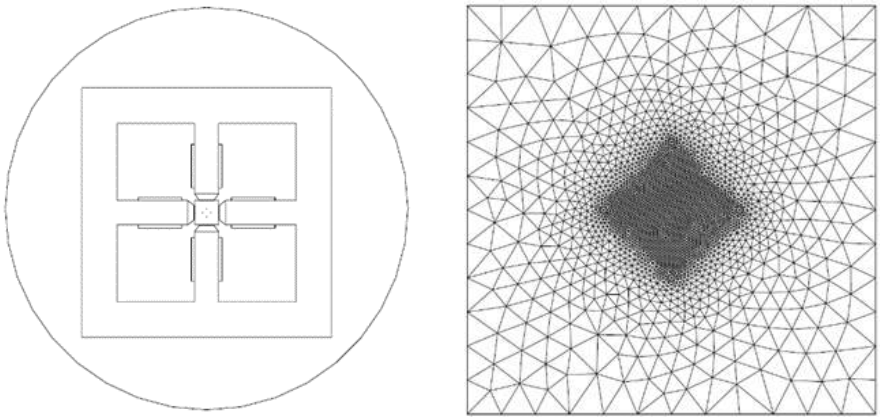

(a) (b)

Fig. 4. Outline of the FE-model(a) and mesh of the probe (b)

functions are used. The area of interest is located in the middle of the probe, where the most homogeneous field can be expected and the magnetic field strength and flux density are evaluated. The coil width of the measuring coils is 20 mm.

The simulations for a sample made of the material FeSi24-50A is carried out at three different excitations, firstly alternating fields in rolling and transverse direction were applied and afterwards a rotational field was applied. The frequency for all simulations is 50 Hz, one period is divided into 120 arbitrary steps.

The projections of the results of measurement and simulation in the rolling and transverse direction for the material FeSi-24-50A show good agreement to the outcomes of the hysteresis model depicted in Figure 5. As expected the simulations with the fixed-point method and the

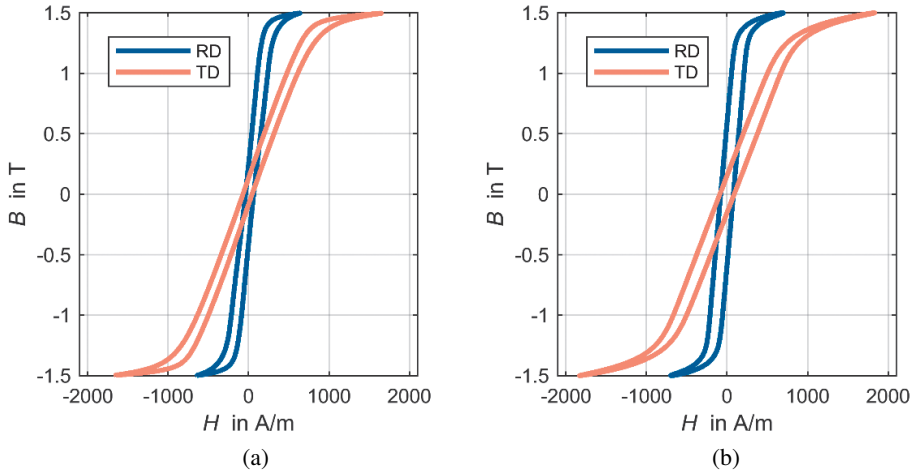

(a) (b)

Fig. 5. Measured (a) and simulated (b) hysteresis curves in RD and TD at 50 Hz

www.czasopisma.pan.pl PAN POLSKA AKADEMIA NAUK www.journals.pan.pl

Newton method lead to the same results. It is clearly shown, that the simulation accurately represents the measured values for the magnetic field strength and flux density.

In Figure 6 the simulation and measurement of the magnetic field strength for a rotating flux density with an amplitude of 1.1 T are shown. The small derivation between the measured H-locus and the simulated one can be found in the fit for the two directions, which is not completely congruent to the uniaxial measured curves. Even though the fit is not optimal in terms of congruency, it can be seen that the PAM is well suited to simulate hysteretic materials

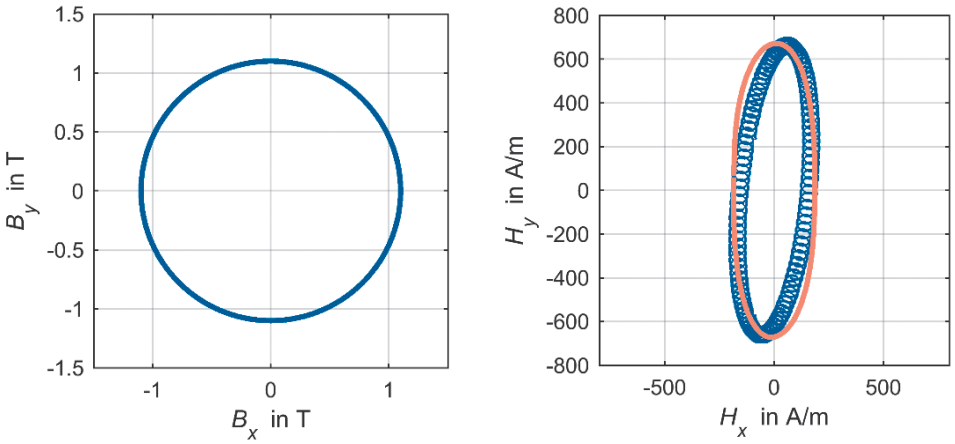

(a) (b)

Fig. 6. Simulated magnetic flux density loci in the middle of the sample (a) and resulting measured (blue circles) and simulated (red line) H-loci (b) at 50 Hz

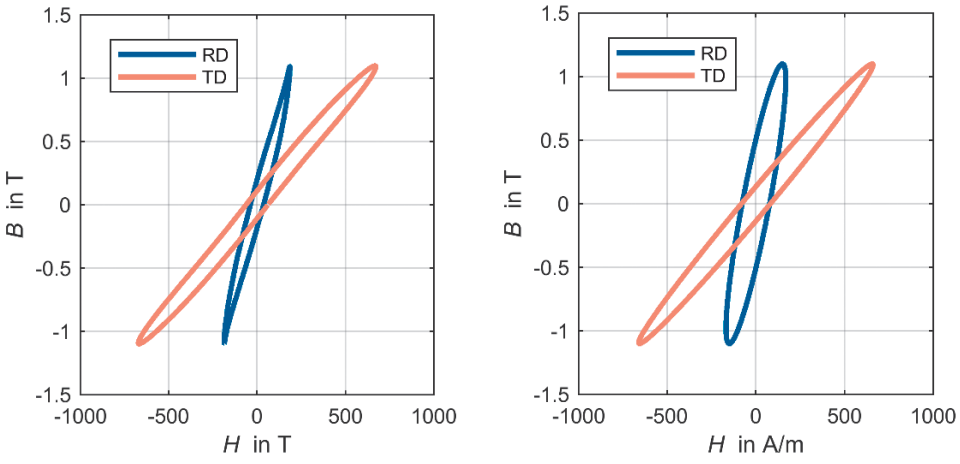

(a) (b)

Fig. 7. Measured (a) and simulated (b) projected hysteresis curves in RD and TD at circular flux density of 1.1 T at 50 Hz

for different excitations, with just one parameter set for each axis. Those parameters can easily be identified from the measurements in rolling- and transversal-direction. It is obvious that the agreement of the curves is accurate, even though the PAM is of simple algebraic nature.

The simulated phase lag between the magnetic field strength and the magnetic flux density is in good agreement with the measurement shown in Figure 8(a). The vectorial relation can be evaluated and depicted for each element in Figure 8(b).

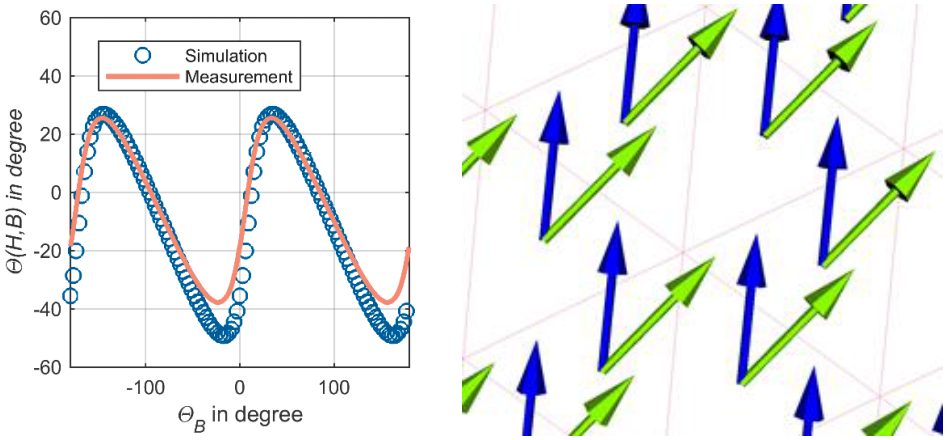

(a) (b)

Fig. 8. Simulated and measured phase lag between H and B-vector (a) and depiction of the simulated vector displacement in the middle of the sample (b)

6. Conclusions

In this paper, a dynamic parameter-based vector hysteresis model is presented and applied to the measuring system used to replicate the measured behavior. Despite the comparatively simple structure of the model, the simulated results of the FE modeling are in good agreement with the measured behavior. Both, the fixed-point and the Newton method provide numerically stable results. The general suitability of the vector hysteresis model as well as the selected numerical methods are clearly proven. In future works the ability of the vector hysteresis model at different levels of flux density and frequency can be evaluated in terms of its suitability to recreate the measured behavior and if necessary adapted. For these studies an examination of the relationship between the model parameters and the respective operation points can be evaluated. Additional effects such as mechanical stress- and temperature dependency can also be considered by evaluations of the parameter dependency with respect to these factors, which influence the magnetic behavior of the examined non-oriented material.

In future work the presented vector hysteresis model will be applied to a rotating electrical machine to analyse its behaviour with focus on global values like torque and losses. The losses determined by the vector hysteresis model will be compared to those obtained by analytical post-processing approaches, like the IEM 5-Parameter Formula [19].

www.czasopisma.pan.pl PAN POLSKA AKADEMIA NAUK www.journals.pan.pl

Acknowledgements

This work was supported by the Deutsche Forschungsgemeinschaft (DFG) within the research projekt number 373150943 *Vector hysteresis modeling of ferromagnetic materials*.

References

[1] Leite J.V., Benabou A., da Silva P.A., Sadowski N., Henneron T., Clénet S., Kuo-Peng P., Piriou F., Batistela N.J., *Analysis of a rotational single sheet tester using 3D finite element model taking into account hysteresis effect*, COMPEL – The international journal for computation and mathematics in electrical and electronic engineering, vol. 26, no. 4, pp. 1037–1048 (2007).

[2] Leite J.V., da Silva P.A., Sadowski N., Batistela N., Peng P.K., Bastos J.P.A., *Vector Hysteresis Under Nonsinusoidal Induction Waveforms: Modeling and Experimentation*, IEEE Transactions on Magnetics, vol. 44, no. 6, pp. 906–909 (2008).

[3] Leite J.V., Ferreira da Luz M.V., Sadowski N., da Silva P.A., *Modelling Dynamic Losses Under Rotational Magnetic Flux*, IEEE Transactions on Magnetics, vol. 48, no. 2, pp. 895–898 (2012).

[4] Thul A., Steentjes S., Schauerte B., Klimczyk P., Denke P., Hameyer K., *Rotating magnetizations in electrical machines: Measurements and modeling*, AIP Advances, vol. 8, no. 5, AIP Advances 8, 56815 (2018).

[5] Fiorillo F., Mayergoyz I.D., *Characterization and Measurement of Magnetic Materials*, Burlington: Elsevier (2004).

[6] Geuzaine C., Steentjes S., Hameyer K., Henrotte F., *Pragmatic two-step homogenisation technique for ferromagnetic laminated cores*, IET Science, Measurement & Technology, vol. 9, no. 2, pp. 152–159 (2015).

[7] Glehn G., Steentjes S., Hameyer K., *Pulsed-Field Magnetometer Measurements and Pragmatic Hysteresis Modeling of Rare-Earth Permanent Magnets*, IEEE Transactions on Magnetics, vol. 54, no. 3, pp. 1–4 (2018).

[8] Mayergoyz I.D., *Vector Preisach hysteresis models (invited)*, IEEE Transactions on Magnetics, vol. 63, no. 8, pp. 2995–3000 (1988).

[9] Matsuo T., Shimasaki M., *Isotropic vector hysteresis represented by superposition of stop hysteron models*, IEEE Transactions on Magnetics, vol. 37, no. 5, pp. 3357–3361 (2001).

[10] Matsuo T., *Anisotropic Vector Hysteresis Model Using an Isotropic Vector Play Model*, IEEE Transactions on Magnetics, vol. 46, no. 8, pp. 3041–3044 (2010).

[11] Sadowski N., Batistela N.J., Bastos J.P.A., Lajoie-Mazenc M., *An inverse Jiles-Atherton model to take into account hysteresis in time-stepping finite-element calculations*, IEEE Transactions on Magnetics, vol. 38, no. 2, pp. 797–800 (2002).

[12] Dlala E., *Magnetodynamic Vector Hysteresis Models for Steel Laminations of Rototing Electrical Machines* (2008).

[13] Hantila F., *Electromagnetic Field in Non-Linear Media*, Balkan Journal of Geometry and Its Applications: BJGA, vol. 4, no. 2 pp. 49–62 (1999).

[14] Mathekga M.E., McMahon R.A., Knight A.M., *Application of the Fixed Point Method for Solution in Time Stepping Finite Element Analysis Using the Inverse Vector Jiles-Atherton Model*, IEEE Transactions on Magnetics, vol. 47, no. 10, pp. 3048–3051 (2011).

www.czasopisma.pan.pl PAN POLSKA AKADEMIA NAUK www.journals.pan.pl

[15] Dlala E., Arkkio A., *Analysis of the Convergence of the Fixed-Point Method Used for Solving Nonlinear Rotational Magnetic Field Problems*, IEEE Transactions on Magnetics, vol. 44, no. 4, pp. 473–478 (2008).

[16] Dlala E., Belahcen A., Arkkio A., *A Fast Fixed-Point Method for Solving Magnetic Field Problems in Media of Hysteresis*, IEEE Transactions on Magnetics, vol. 44, no. 6, pp. 1214–1217 (2008).

[17] Gyselinck J., Dular P., Sadowski N., Leite J., Bastos J.P.A., *Incorporation of a Jiles-Atherton vector hysteresis model in 2D FE magnetic field computations*, COMPEL – The international journal for computation and mathematics in electrical and electronic engineering, vol. 23, no. 3, pp. 685–693 (2004).

[18] Kruttgen C., Steentjes S., Glehn G., Hameyer K., *Parametric homogenized model for inclusion of eddy currents and hysteresis in 2-D finite element simulation of electrical machines*, IEEE Conference on Electromagnetic Field Computation (CEFC) November 2016, Miami, FL, p. 1 (2017), DOI: 10.1109/TMAG.2017.2660460.

[19] Eggers D., Steentjes S., Hameyer K., *Advanced Iron-Loss Estimation for Nonlinear Material Behavior*, IEEE Transactions on Magnetics, vol. 48, no. 11, pp. 3021–3024 (2012).